A&A 638, A120 (2020)
https://doi.org/10.1051/0004-6361/202037594

Astronomy & Astrophysics

Searching for the near-infrared counterpart of Proxima c using multi-epoch high-contrast SPHERE data at VLT⋆,⋆⋆

R. Gratton[1], A. Zurlo[2,3,4], H. Le Coroller[4], M. Damasso[5], F. Del Sordo[6,7], M. Langlois[8,4], D. Mesa[1], J. Milli[9], G. Chauvin[10,11], S. Desidera[1], J. Hagelberg[12], E. Lagadec[13], A. Vigan[4], A. Boccaletti[14], M. Bonnefoy[10], W. Brandner[15], S. Brown[15], F. Cantalloube[15], P. Delorme[10], V. D'Orazi[1], M. Feldt[15], R. Galicher[14], T. Henning[15], M. Janson[16], P. Kervella[13], A.-M. Lagrange[10], C. Lazzoni[1], R. Ligi[17], A.-L. Maire[15,18], F. Ménard[10], M. Meyer[19], L. Mugnier[20], A. Potier[14], E. L. Rickman[12], L. Rodet[10], C. Romero[10], T. Schmidt[14,21], E. Sissa[1], A. Sozzetti[5], J. Szulágyi[22], Z. Wahhaj[9], J. Antichi[23], T. Fusco[20], E. Stadler[10], M. Suarez[24], and F. Wildi[12]

(Affiliations can be found after the references)

Received 28 January 2020 / Accepted 14 April 2020

ABSTRACT

Context. Proxima Centauri is the closest star to the Sun and it is known to host an Earth-like planet in its habitable zone; very recently a second candidate planet was proposed based on radial velocities. At quadrature, the expected projected separation of this new candidate is larger than 1 arcsec, making it a potentially interesting target for direct imaging.

Aims. While identification of the optical counterpart of this planet is expected to be very difficult, successful identification would allow for a detailed characterization of the closest planetary system.

Methods. We searched for a counterpart in SPHERE images acquired over four years through the SHINE survey. In order to account for the expected large orbital motion of the planet, we used a method that assumes the circular orbit obtained from radial velocities and exploits the sequence of observations acquired close to quadrature in the orbit. We checked this with a more general approach that considers Keplerian motion, called K-stacker.

Results. We did not obtain a clear detection. The best candidate has signal-to-noise ratio $(S/N) = 6.1$ in the combined image. A statistical test suggests that the probability that this detection is due to random fluctuation of noise is <1%, but this result depends on the assumption that the distribution of noise is uniform over the image, a fact that is likely not true. The position of this candidate and the orientation of its orbital plane fit well with observations in the ALMA 12 m array image. However, the astrometric signal expected from the orbit of the candidate we detected is 3σ away from the astrometric motion of Proxima as measured from early *Gaia* data. This, together with the unexpectedly high flux associated with our direct imaging detection, means we cannot confirm that our candidate is indeed Proxima c.

Conclusions. On the other hand, if confirmed, this would be the first observation in imaging of a planet discovered from radial velocities and the second planet (after Fomalhaut b) of reflecting circumplanetary material. Further confirmation observations should be done as soon as possible.

Key words. planets and satellites: detection – planets and satellites: individual: Proxima c – stars: individual: Proxima – planets and satellites: terrestrial planets – instrumentation: high angular resolution – techniques: image processing

1. Introduction

Proxima Centauri (hereafter Proxima) is the closest star to the Sun (1.3012 ± 0.0003 pc: Benedict et al. 1999; van Leeuwen 2007; Gaia Collaboration 2018) and its planetary system is among the most likely to allow a detailed investigation of an Earth-like planet. Anglada-Escudé et al. (2016) discovered a close-in Earth-like planet, Proxima b, using radial velocities (RV). This planet was confirmed by Damasso & Del Sordo (2017) and a more accurate estimate of the mass of $m_b \sin i_b = 1.0 \pm 0.1\ M_\oplus$ was obtained by Damasso et al. (2020). This planet is in the habitable zone, but it is too close to the star for direct imaging with current instrumentation (projected semi-major axis $a \sim 37$ mas). In the near future, a combination of high-resolution spectroscopy and high-contrast imaging might facilitate the detection of its signal and ultimately the study of the composition of its atmosphere (Snellen et al. 2015; Lovis et al. 2017). Through additional RVs, Damasso et al. (2020) found evidence of a second planet (Proxima c) with a minimum mass of $5.8 \pm 1.9\ M_\oplus$ on a roughly circular orbit with period of 1900^{+96}_{-82} days $= 5.21^{+0.26}_{-0.22}$ yr, and semimajor axis of 1.48 ± 0.08 au, corresponding to a maximum angular separation of 1.14 ± 0.06 arcsec. This planet is compatible with the upper limit set from astrometry (Benedict et al. 1999; Lurie et al. 2014). Hereafter, we use the epoch, period, and semimajor axis of the circular orbit solution by Damasso et al. (2020) to fine-tune our search for Proxima c.

Given its large apparent separation from the star, direct detection of Proxima c might be perhaps feasible, though difficult,

⋆ The reduced images are only available at the CDS via anonymous ftp to cdsarc.u-strasbg.fr (130.79.128.5) or via http://cdsarc.u-strasbg.fr/viz-bin/cat/J/A+A/638/A120

⋆⋆ Based on data collected at the European Southern Observatory, Chile (ESO Programs 095.D-0309, 096.C-0241, 096.D-0252, 097.C-0865, 198.C-D0209, 099.D-0098, 099.C-0127.

owing to the large expected contrast. In this paper we report on the search of the optical counterpart of the candidate planet Proxima c in a series of observations acquired from the SPHERE (Beuzit et al. 2019) guaranteed time observations (GTO). This data set was obtained with the aim of measuring the mass of Proxima from the relativistic deflection of the apparent motion of background stars (Zurlo et al. 2018a). Mesa et al. (2017) performed an analysis of the limits in the mass of possible companions from data available at the time. The mass limit obtained by Mesa et al. (2017) is an order of magnitude or more higher than the most probable mass for the candidate planet proposed by Damasso et al. (2020). However, there are a number of additional facts that justify a reanalysis of the data: (i) Mesa et al. (2017) used only a subset of the data that is currently available. We later acquired new data sets that were obtained in better atmospheric conditions and are therefore of higher quality. Furthermore, given the very large expected orbital motion, Mesa et al. (2017) did not combine results from different epochs and used only the best data set for their analysis. We can now try to combine results obtained at different epochs in a deeper search. (ii) Since there was no candidate at the time, the search was completely blind. In order to reduce the false alarm probability (FAP), Mesa et al. (2017) had to adopt a conservative detection threshold that is the usual 5σ level used in direct imaging surveys. Availability of a spectroscopic orbit allows a very significant reduction of the search area, relaxing this condition substantially. (iii) Mesa et al. (2017) considered only planets shining by their internal energy; while reflection of stellar light by the planet itself is not expected to be larger than a few 10^{-9} for the case of Proxima c, it might be enhanced, for example, by the presence of debris circumplanetary rings (see, e.g., Arnold & Schneider 2004) or dust around the planet as proposed for Fomalhaut b (Kalas et al. 2008; Kennedy & Wyatt 2011). Thanks to the additional knowledge provided by the spectroscopic orbit and considering the more specific cases described above, we endeavor to reanalyse the detectability of this counterpart. As shown in the remaining part of this paper, current high-contrast data still do not provide a robust detection of Proxima c. However, since for practical reasons we have no opportunity to observe again Proxima with high-contrast imagers in 2020, we present our analysis in a paper because we think it may be useful to others, for example, in preparation and comparison with future high-contrast imaging or *Gaia* or ALMA observations. In this paper we also describe methods that can be useful in similar analysis for this and other objects.

Given the distance of Proxima and the length of the proposed period for Proxima c, the planet is expected to move rapidly along its orbit around the star (a few mas day^{-1}). This must be taken into account when combining results from different epochs. We considered two possible approaches. The first uses the slower apparent motion of the candidate close to expected orbital quadrature and is similar to that considered by Mawet et al. (2019) in their search for the planet around ϵ Eri; the first guess on the orbital properties obtained with this approach is then used as a guide for identification of the possible planet signal at other epochs. The second uses K-stacker (Le Coroller et al. 2015, 2020; Nowak et al. 2018), that is a more generic code for identifying a sub-threshold signal in multiple observations of an orbiting object. However, K-stacker is only used in a limited way, essentially as a confirmation of the result we obtained with the other approach; we leave a more extensive use of this approach for the future. The paper is structured as follows: in Sect. 2 we describe the observations; in Sect. 3 we outline the methods used in the search and present the results; in Sect. 4 we discuss our findings in the context of Proxima c; conclusions and suggestions for further work are in Sect. 5.

2. Observations

We list the epochs of the SPHERE GTO observations of Proxima in Table 1. For each epoch, we also give the phases corresponding to the RV orbit of Proxima c as well as the expected separation along the major axis of the projected orbit. We note that the orbit proposed by Damasso et al. (2020) is circular. The listed values are the real separation only for an inclination $i = 90$ degrees or for a phase of 0.25 or 0.75. For a non-edge-on orbit the actual projected separation is larger for most orbital phase angles.

Since Proxima c is expected to be at a separation larger than 1 arcsec from the star for a large fraction of its orbit, the search should be done over a large field of view. We then need to consider data acquired with the IRDIS dual band imager (Dohlen et al. 2008), which has a roughly square field of view with a side of about 11 arcsec, while at best the planet should be in the field of view of the Integral Field Spectrograph (IFS: Claudi et al. 2008) for only a fraction of the observations. In order to describe the quality of the observation at each epoch, we give in Table 1 the 5σ limiting contrast at 0.5 arcsec obtained with IFS using the deepest analysis method we tried, which was principal component analysis (PCA; with simultaneous angular and spectral differential imaging: Marois et al. 2006; Soummer et al. 2012; Amara & Quanz 2012; Mesa et al. 2015). All observations were acquired in the IRDIFS mode, that is observing with IRDIS in the H2/H3 dual-band imaging filters (Vigan et al. 2010) and with IFS in the *Y-J* mode.

3. Analysis and results

3.1. Data preparation

The reduction of data for individual epochs was performed as described in Zurlo et al. (2018a) and makes use of the DRH pipeline (Pavlov et al. 2008) as implemented at the SPHERE Data Center (Delorme et al. 2017). Zurlo et al. (2018a) provide more details on the preprocessing and final products of the reduction. We used the images obtained after application of monochromatic PCA to the final images for this analysis (average of those obtained with the H2 and H3 filter of IRDIS), and we removed the background stars inside a radius of 5 arcsec. Background stars that have a signal above the detection threshold signal-to-noise ratio ($S/N > 5$) in individual images were already identified in the analysis by Zurlo et al. (2018a). The values for pixels for which there were signals from the background stars were replaced by the median of the surrounding background in the data cube prior to PCA analysis; there were three objects that had signals from background stars in the portion of the images considered in this paper. While removing most of the signal related to these sources, this procedure may however leave residual "ghosts" at $S/N \sim 2$–3 in the corrected images. In addition there are images of two faint background stars ($3 < S/N < 5$, that is, below the threshold for detection in the individual images) still present in the images. These stars can be separated from noise spikes of similar intensity comparing different images because they move very rapidly ($\sim$10 mas day^{-1}) over the observed field of view, but their relative positions are constant. One of these stars is out of the considered region in

Table 1. SPHERE Proxima observations.

MJD	Date	Exp.time s	Seeing arcsec	Rotation degree	Contrast mag	Phase c	Sep ($i = 90$ degree) mas	Note
57 112	2015-03-31	576	0.95	3.2	12.18	0.6459	896	
57 406	2016-01-19	4480	2.20	25.7	13.31	0.8007	1088	
57 436	2016-02-18	1760	1.86	13.5		0.8163	1050	Poor
57 448	2016-03-01	3392	0.78	22.6	12.57	0.8226	1031	
57 475	2016-03-28	4000	2.08	25.7	13.88	0.8370	984	
57 494	2016-04-16	3840	0.62	28.7	12.65	0.8496	946	
57 830	2017-03-19	2048	1.10	11.5	13.88	0.0237	146	
57 919	2017-06-14	2720	1.88	20.9	12.65	0.0706	467	
58 222	2018-04-13	4320	0.58	29.3	14.23	0.2301	1127	
58 227	2018-04-18	4480	0.55	30.0	14.00	0.2327	1130	
58 244	2018-05-05	3840	0.65	25.7	14.31	0.2417	1137	
58 257	2018-05-18	3840	0.40	25.7	14.36	0.2484	1139	
58 288	2018-06-20	3840	1.70	24.1	13.88	0.2648	1137	
58 588	2019-04-15	4608	0.47	25.8	14.55	0.4221	560	
58 621	2019-05-17	1920	0.91	26.6	14.02	0.4401	449	

Notes. Contrast is measured at 0.5 arcsec on IFS images; phase c is the phase of planet c from the spectroscopic orbit.

the last epoch. In both cases, ghosts of bright and faint background stars may be visible in the median image depending on how their signals combine with local noise at other epochs. Concerning this point, we notice that while at large separation from the star the noise is not strongly correlated pixel-to-pixel, the S/N from a background star is >2 over several (~10) adjacent pixels because the detector is over-sampled. The probability that a signal at more than $S/N = 2$ appears at the final median image in the position of a background star depends on the noise distribution; we tested this by considering the fraction of pixels that have at least two cases with $S/N > 2$ over four extractions out of five, so that the median value combined with the strong residual in the fifth image is $S/N > 2$, for at least one pixel over all the pixels with $S/N > 2$ corresponding to a background star (that we assumed in this work to be 10). We found that this probability is ~5% if we assume a Gaussian noise distribution; it is larger in a more realistic case where the probability of having peaks at more than 2σ is larger than for a Gaussian distribution. We conclude that having two such cases observed in the median images (as observed, see Fig. 1) is not unlikely.

3.2. Observations acquired near quadrature

For a circular orbit with known conjunction epoch, period, and semimajor axis, the planet position at each epoch depends on two parameters: the inclination i and the position angle (PA) of the orbit. Combining the images at generic epochs requires raising the threshold for detection to avoid false alarms. Even with small variations of i and Ω, the longitude of the ascending node would lead to quite different predictions about the location of the planet at different epochs; combined with the unknown value of orbital PA and the fact that the real orbit is likely not exactly circular, this implies the need to search over a substantial fraction of the available images. However, close to quadrature, that is at phases of 0.25 and 0.75 according to the convention adopted by Damasso et al. (2020), the difference between the real separation and that along the major axis is negligible for any value of the inclination for a circular orbit. This implies that if we only use observations taken close to this phase, we may limit our search to a narrow ring around the star (see Mawet et al. 2019 for a similar argument). In addition, around quadrature the variation with time of the planet PA along the orbit depends on the inclination at which the orbit is observed, and has an upper limit because the

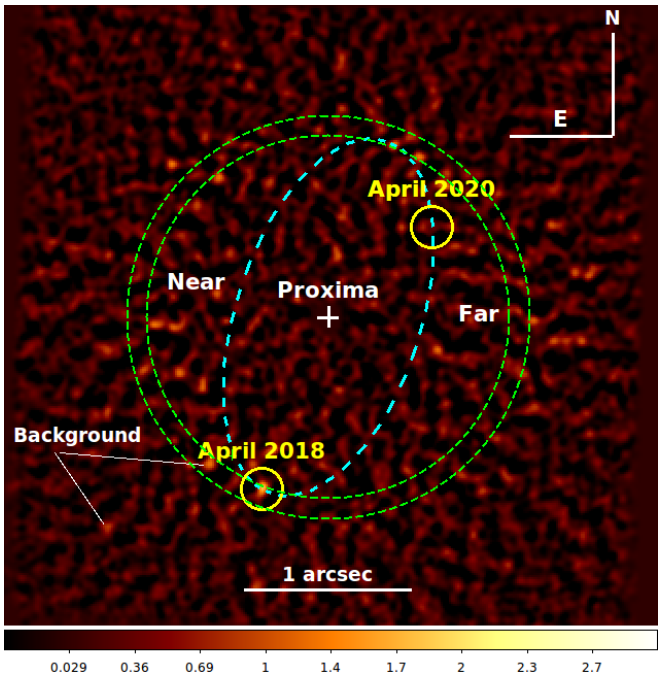

Fig. 1. Median of the five epochs of Proxima acquired near quadrature in 2018 (MJD 58222, 58227, 58244, 58257, 58288), combined assuming an inclination of i = 120 degree. Individual images were rotated to take into account orbital motion with respect to the reference epoch (MJD = 58 222). The north and east positions are then correct for that epoch alone. The search area for c is the ring between the two green dashed circles, with inner radius of 1080 mas and outer radius of 1200 mas. The yellow circles denote the best candidate at the epoch of observation (that is MJD = 58 222, 2018-04-13) and at mid-April 2020, providing an idea of the speed and direction of the orbit. The cyan dashed line represents the orbit of the candidate planet on the sky plane. Two faint background stars are still visible in this image. The color bar is the median S/N over the five epochs.

apparent orbital speed should be compatible with Kepler's third law (assuming a mass of 0.12 $M_\odot$ for Proxima: Mann et al. 2015). This leads to a small number of possible combinations (essentially rotations) of the images acquired at different epochs that are compatible with Keplerian motion, and then substantially restricts the volume of the phase space where the search of the Proxima c signal should be done.

Luckily, in 2018 we acquired a sequence of five good data sets, spanning the limited range in phase between 0.2301 and 0.2648, which are all very close to quadrature. The expected span of separation of planet c image from the star is very narrow, between 1.127 and 1.139 arcsec. This is much narrower than the error bar on the semimajor axis from the spectroscopic orbit (1.137 ± 0.061 arcsec) and the full width at half maximum (FWHM) of the diffraction peak of SPHERE images (~0.035 arcsec). We may then assume that during all these epochs, the candidate is at a nearly constant separation, and the planet PA changes with time because of the projection of the circular motion related to the inclination of the orbit. We note that during these epochs, we expect the candidate to be out of the IFS field of view. Hence, we should search for it in the IRDIS images.

Following the previous discussion, we combined the S/N maps extracted from the observations acquired in 2018 (spanning about two months) by rotating the images with respect to the first. This rotation is that expected owing to the apparent motion of the planet for different values of the inclination. These S/N maps were obtained with the same procedure presented in Zurlo et al. (2014), after subtracting obvious background stars. We then made a median of the results to reduce sensitivity to possible residuals of background objects. We repeated this procedure for different values of the inclination with a step of 9 degrees in inclination (that is 1.14 degree in field rotation) from 0 to 180 degrees (that is, 21 steps). This step is small enough to ensure that whatever is the correct inclination, we have at least one combination of images for which the difference between the real and model orbital motion leads to a shift of the candidate planet image by less than one pixel (the scale is 12.25 mas pixel^{-1}) over the epoch range covered by the 2018 observations. This is about one-third of the FWHM of point-source images, which is about three pixels.

In each combined image, we then searched for the highest peak in the ring with separation of 1133 ± 61 mas, where we expect the companion is close to quadrature; to reduce random variations, we smoothed these combined images using a current median of 3 × 3 pixels, that is, the expected FWHM of point sources. However, we obtained the same result with different values of the smoothing parameter in the range between 1 (that is, no smoothing at all) to 7 pixels.

The best candidate that we found with this process is at a separation of 1072 mas (at the inner edge of the search area) and the PA = 157.90 degrees (for the epoch JD = 58 222.20). This is obtained for an inclination of i = 120 degrees (see Fig. 1), which corresponds to a counter-clockwise motion. Once combined with RVs, this motion implies that the near side of the orbit is on the NE and the far side of the orbit is on SW. We note that the peak corresponding to the candidate found for this angle is the highest in the whole image even though the area within the ring covers less than 6% of the surveyed image. The detection is at a S/N of 6.1 in the median image, estimated as the ratio of the peak S/N to the standard deviation over a 100 × 100 pixel area at a similar separation from the star. The median value of the S/N values over the images at individual epochs is 3.4. The second highest peak in the median image is at $S/N = 4.8$ and there are only two other peaks above $S/N = 4$, but they are all out of the search area.

In Fig. 2 and Table 2, we show the results from the individual epochs. From this data, the S/N for the candidate are quite uniform over the different epochs; although the number of epochs is not large, this is not what expected for a background source, which should not share the large proper motion with Proxima and hence have a high S/N only in a single image. On the other hand, it is clear that only by combining several images we can hope to achieve a reliable counter-identification.

3.3. Reliability of this detection

Whether or not we can be confident that the candidate found using the previous analysis is the counterpart of Proxima c is not an easy question to answer. We considered the issue from different point of views.

3.3.1. Source as a possible random fluctuation

First, the probability that this detection is a false positive is possibly low is suggested by the following argument. As mentioned above, the area within the ring is only 6% of the area of the S/N maps (radius of 2 arcsec), and the candidate peak has the highest S/N in the whole map. In addition, we note that each relative rotation we applied to the images for individual epochs corresponds to creating a new noise realization in the combined image; so far the rotation between different images is large enough to shift the noise peaks more than their correlation length, that is approximately the FWHM of the point spread function. For better statistics of the maximum S/N obtained for random peaks, we then extended the rotation over the whole range of 360 degrees. We also considered values that are incompatible with Keplerian motion, which would limit rotation to the range from −12 degrees to +12 degrees; we did this with a step of 3 degrees to ensure that results obtained for each rotation angle are independent from each other. In this way we searched the entire parameter space, and the subthreshold solution happens to line up with the parameter space where an orbit is detected. Over all these combinations, we found only one case anywhere in the image where the maximum S/N is higher than for the candidate over the whole combined S/N maps.

There are 1/120 random instances of signal this high, but the search area is 16 times smaller, so the likelihood of a random signal this high is 1/(120 × 16), that is 1 odd over 1920 cases. We may then use a binomial distribution and assume that the number of extractions is equal to the number of independent angles considered for the search of Proxima c (nine) and that the probability of a random result for a single extraction is 2/1920 = 0.1%; this also counts the possible detection of Proxima c candidate because we should consider the possibility that this detection is a random result. The result is a probability of about 0.9% of finding by chance a peak as strong as that observed within the search area (distance from the star and field rotation) considered. Statistics dealing with one detection are always tricky. For instance, this test assumes that the distribution of noise in the S/N maps is the same over the whole field of view, which is likely not true close to the star (see, e.g., Mawet et al. 2014 and references therein), and that noise realizations are really independent from each other, possibly not true close to the star. It is then possible that the FAP is higher than estimated by this test. Anyhow, this low probability suggests that we found an interesting candidate for the optical counterpart of Proxima c.

3.3.2. Source in a region of high background noise

Another point of possible concern is the following. In the image obtained at JD 58244 there appears to be a feature starting to

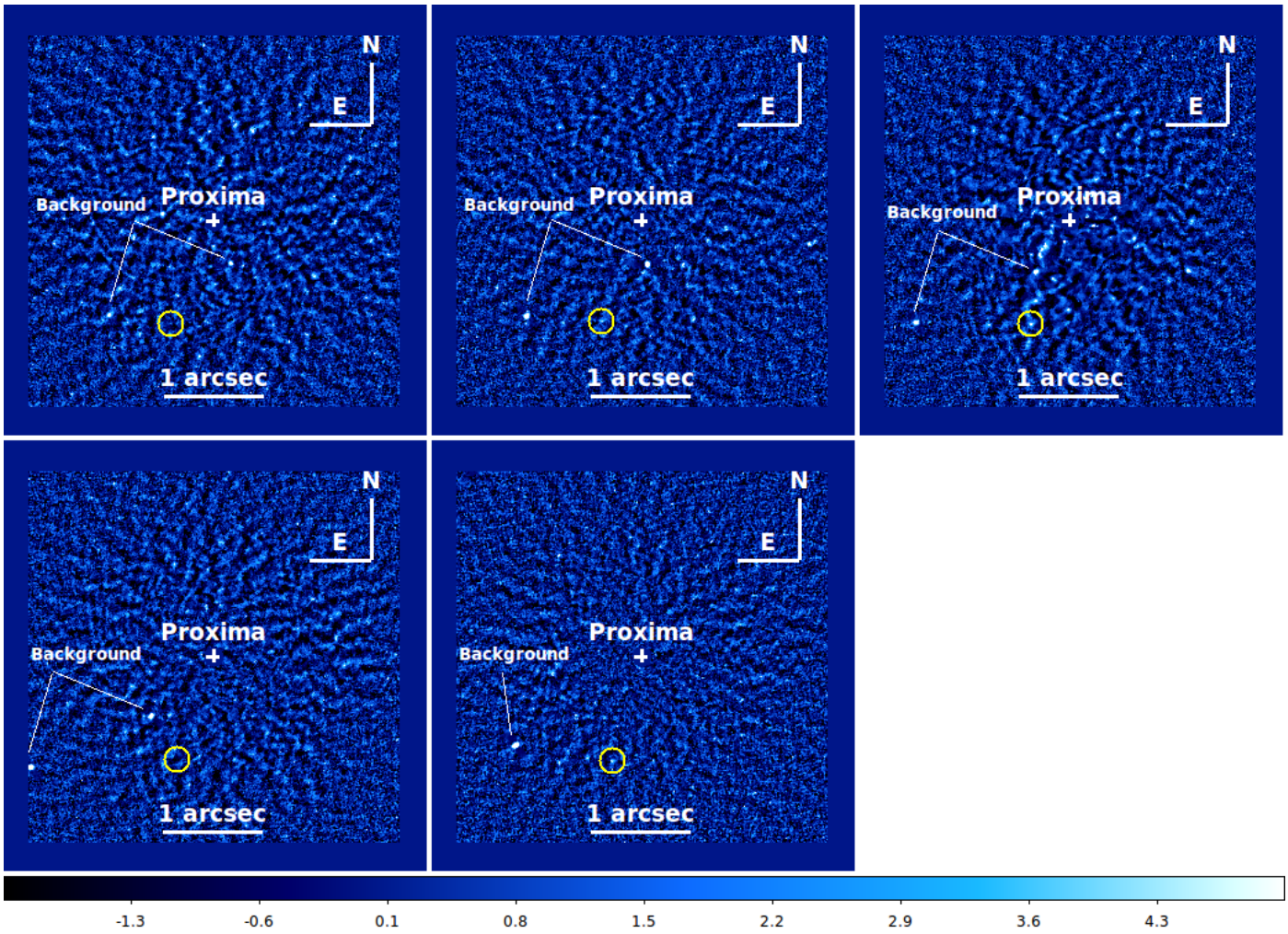

Fig. 2. Individual S/N maps for the five 2018 epochs. *From left to right, top row*: MJD 58 222, 58 227, 58 244; *bottom row*: 58 257, 58 288. The candidate counterpart of Proxima c is circled. Some bright background sources not subtracted from the individual images are shown. However, these move rapidly because of the large proper motion of Proxima, so they are not as clear in the median image of Fig. 1. The color bar is the S/N. S/N detection is at $S/N = 2.2$ (MJD 58 222), 3.4 (MJD 58 227), 5.9 (MJD 58 244), 1.2 (MJD = 58 257), and 4.1 (MJD 58 288).

Table 2. Measures of the counterpart candidate to Proxima c at the various epochs.

MJD	PA (degree)	Sep (mas)	*S/N*
57 406	0.08	870	3.7
57 830	100.82	809	1.2
58 222	157.13	1104	2.2
58 227	158.19	1068	3.4
58 244	159.36	1092	5.9
58 257	160.83	1087	1.2
58 288	164.47	1079	4.1
58 588	218.67	802	1.6
58 621	225.13	767	3.1

the left of Proxima Cen and passing through the position where the Proxima c candidate signal is claimed. This is the highest S/N detection of the companion, and the possibility that the detection is a peak in this linear feature (presumably a correlated noise feature) should be considered. We then had a closer look at this structure. The structure includes both a background object and the possible image of Proxima c candidate. To avoid biasing the results due to these features, we only considered the region between the features and avoiding regions closer than 5 pixels to either of them. This comparison region includes about 600 pixels. The average S/N value within it is 0.10 ± 0.05, that is, slightly different from zero (i.e., the expected value) but only at about 2σ level. The root mean square (rms) within this region is 1.25 ± 0.05 (in noise units). The region is then slightly more noisy than the whole image. The significance of these two results is not clear because this area was picked out among the images obtained at different epochs exactly because it looked a bit different at eye inspection. However, the differences in both the mean value and rms scatter are much lower than the S/N measured for the candidate position (that is, 5.9). On the other hand, this result suggests that the S/N obtained for the possible position of Proxima c candidate in this image might be overestimated by some 25% because the local noise is possibly underestimated. This may contribute to explaining why this value deviates so much from the typical value of about 3 obtained at other epochs. In any case, the impact of this result in our conclusion is marginal because we are using median values over the different images. If we neglect this image, the median value is reduced from 3.4 to 2.8.

3.3.3. Expectation of S/N fluctuation

A more general concern is whether the observed fluctuations of the S/N among different observations are compatible with the hypothesis of a real signal.

In general, we expect that there is a scatter in the S/N detections over different visits, even if the signal and noise were constant. This is due to the actual realization of noise in the individual observations. If the S/N is correctly evaluated, which is not an easy task in high-contrast imaging (see also the discussion above), we expect that if the noise is only due to the background, the rms of the S/N in single observation should be 1, and its measure should be 1.0 ± 0.3 because we are considering nine epochs. On the other hand, if the noise is mainly due to the source itself, the rms of the S/N should be roughly equal to $\sqrt{(\langle S/N \rangle)} = 1.7 \pm 0.3$. If we consider all the values listed in Table 2, the mean value for the S/N is 2.9 with an rms equal to 1.5 ± 0.5; the rms reduces to 1.3 ± 0.4 if the S/N for epoch 58257 is reduced to 4.6, as discussed above. This value is intermediate between that expected for background and source noise dominated cases, and is compatible with the two cases. This looks appropriate for this region of the image, further from the star than the high noise ring related to the outer working angle of the adaptive optics. Given the uncertainties in these determinations, this result is reasonable, although of course we cannot exclude the possibility that noise is slightly underestimated (or simply that signal and/or noise are not constant).

We might also expect that there should be some correlation of the S/N of detection with the (nominal) limiting magnitude (under the hypothesis that the signal is constant). There is only a very weak negative correlation (Persson correlation coefficient $r = -0.155$) and we aim to determine if this is unexpected. First, we note that the 2016 data sets, which are of much lower quality, are combined in Table 2. If we combine the limiting value for each epoch quadratically taking into account they are logarithmic quantities, the appropriate limiting magnitude for the combined 2016 observation should be read as 14.12 mag; this is very similar to the average for the other epochs listed in Table 2 (14.16 mag). Second, the values of the nominal limiting magnitudes are also affected by uncertainties and do not greatly change within the sample. The rms of the values is 0.23 mag; this value is close to the uncertainties in the photometric zero points in observations with SPHERE (0.18 mag). This point is discussed at some length in Langlois et al. (in prep.), in which we discuss the accuracy of the photometry of the SHINE survey. This uncertainty is related to the variations of the Strehl ratio of the observations obtained with the star out of the coronagraphic mask, which is used to determine the zero point of the photometry, to the science exposure with the star behind the coronagraph. We note that this is likely an underestimate of uncertainties in the limiting contrasts because it neglects any other effect (such as errors in the estimate of correct noise level).

If we combine uncertainties in the limiting magnitude and in the S/N of the source, we really do not expect that the correlation of the S/N of detection with the (nominal) limiting magnitude should be obvious in the data. To show this, we considered the case in which there is a real signal as given by the mean value of the observations (contrast of 14.75 mag) and that the observations have a real limiting magnitude with a Gaussian distribution with a mean value of 14.15 mag and an rms scatter of 0.15 mag over a set of nine observations. We then added realistic Gaussian noise both in the S/N estimate ($\sigma = 1.5$) and on the limiting magnitude estimate ($\sigma = 0.18$ mag), reproducing the observed scatter in S/N values and limiting magnitude (0.23 mag). We then repeated this procedure 10 000 times and looked for how many cases the Pearson correlation coefficient between limiting magnitude and S/N is below the observed value of $r = -0.155$. We found that if there is a real signal, in the presence of realistic noise estimates, in 20% of the cases we should have found a negative correlation stronger than we observed between limiting magnitude and S/N.

Summarizing, these arguments do not show that we detected Proxima c, but simply that the S/N fluctuations among different observations are compatible with this hypothesis, even assuming that the signal is constant.

3.4. Results obtained with K-stacker

K-stacker (Le Coroller et al. 2015, 2020; Nowak et al. 2018) is a method of observation and reduction that consists in combining high-contrast images recorded during various nights, accounting for the orbital motion of the putative planet that we are looking for, and then looking for peaks in the final S/N maps obtained in this way. The K-stacker approach takes a long time to compute because this brute-force algorithm searches simultaneously for new planets and for their orbital parameters (Le Coroller et al. 2020). A full K-stacker solution using all epochs is not included in this paper; we plan to present it in a forthcoming paper. Le Coroller et al. (2020) show how it is important that a stacking approach is used on data of homogeneous (high) quality; for this reason, for this first approach we used only the 2018 epochs and we limited the exploration to those range of orbital solutions that are consistent with the spectroscopic orbit ($1.2 < a < 1.5$ au and $e < 0.1$). We assumed a stellar mass of $m = 0.135\ M_{\odot}$, that is, the mean of the values given by Mann et al. (2015) and Zurlo et al. (2018a). The mass used in the K-stacker computation is not the best value, but K-stacker computations demand a lot of time. Since this assumption does not not play a central role in the paper, we prefer to avoid repeating these computations.

K-stacker always gives a family of solutions (Le Coroller et al. 2020). The solution we obtained with the highest S/N is the same peak found in the quadrature analysis described in the previous subsection and also the orbital parameters are very similar ($a = 1.47$ au, $i = 122$ degree, $\Omega = 165$ degree, and a moderate eccentricity of $e = 0.066$). The value of the $S/N = 4.1$ is lower than in the quadrature analysis, but since it is computed using a different algorithm there is no reason for the two values to coincide exactly. More importantly, the S/N value is below the threshold usually considered for reliable orbits (see Nowak et al. 2018; Le Coroller et al. 2020). We have to consider that, compared with the cases considered in those papers, in the present case we are exploring only a limited region of the possible parameter space where Keplerian solutions may fall, reducing the FAP. Overall, while this result is not a really independent confirmation of the detection of c on SPHERE data, the result at least confirms that the family of solutions considered in the previous subsection best matches the 2018 SPHERE observations in the framework of orbits, thereby satisfying the constraints set by the spectroscopic orbit.

3.5. Other epochs

Only two observations of rather poor quality were acquired in 2017 when the planet was likely at a smaller separation from the star and possibly close to the noisy region around the outer working angle of the adaptive optics. On the other hand, we may look for the candidate derived from 2018 data in the sequence of observations acquired in 2016. This data set includes several

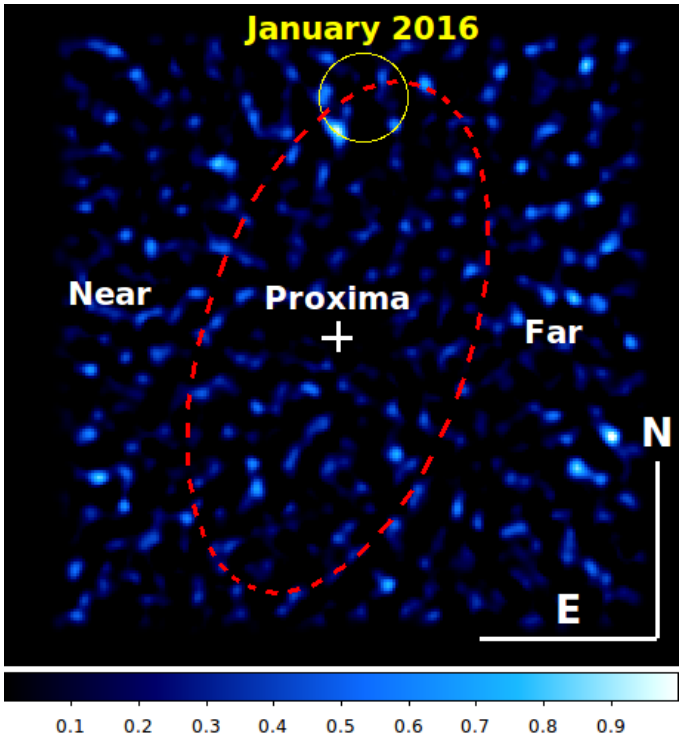

Fig. 3. Median of five 2016 observations, shifted to the first of these epochs (January 2016: JD = 57 406) according to the circular orbit suggested by 2018 observations (red ellipse). The yellow circle is the expected position at that epoch; the radius of this circle is ∼180 mas. The color bar is the median S/N over the five epochs.

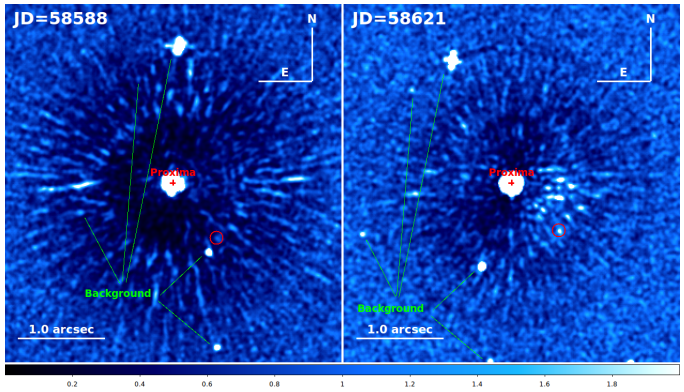

Fig. 4. Signal-to-noise maps for the two epochs acquired in 2019 (JD = 58 588 and 58 621). The red circles indicate the possible counterparts of Proxima c at these epochs. Background stars are also shown. The color bar is the S/N.

Table 3. Proposed orbital parameters.

Parameter	Spectroscopic orbit	Circular orbit	Elliptical orbit
Period (yr)	5.20 ± 0.26	5.20	5.08 ± 0.34
Epoch of quadrature (JD)	58260 ± 100	58260	58165 ± 80
Eccentricity	0.0	0.0	0.080 ± 0.044
Semimajor axis (arcsec)	1.14 ± 0.06	1.072	1.02 ± 0.06
Semimajor axis (au)	1.48 ± 0.08	1.40	1.33 ± 0.08
Ω (degrees)		164	150 ± 7
ω (degrees)			−2 ± 34
Inclination (degrees)		120	137.3 ± 6.2

observations, but they were not acquired close to quadrature and are of lower quality due to worse sky conditions. We retrieved the five best of these images - those from January to April 2016 (MJD = 57 406, 57 436, 57 448, 57 475, 57 494). We then combined these images by shifting them to the first epoch as expected from the circular orbit that best matches the 2018 observations and then finding the median; this procedure is similar to that described by Showalter et al. (2019) in their search for the seventh moon of Neptune. The result is shown in Fig. 3. The expected position coordinate does not have a maximum. The closest peak ($S/N = 3.7$, the second highest peak in the whole S/N map) is at about 15 pixels (∼180 mas) from the expected position. There could be three reasons for this: (i) the candidate we retrieved in 2018 is not the counterpart of Proxima c; (ii) Proxima c was fainter in 2016; this is not unlikely because we expect that at this epoch visibility was less favorable because the planet is possibly on the near side of the orbit and then shows a larger fraction of its dark side; and (iii) we did not assume the correct orbit. For instance, if we had only adopted a period at the longest edge of the error bar, leaving aside other uncertainties such as a small (but not zero) eccentricity, we would have expected Proxima c to be at about 100 mas from the expected position for the nominal period. On the other hand, we might assume that this local maximum is a real detection of Proxima c (yielding a position of dRA = 1 mas and dδ = 870 mas, at JD = 57 406).

We also explored the two epochs acquired in 2019 (JD = 58 588 and 58 621) that are of fairly good quality (Fig. 4). Since these epochs were acquired far from quadrature, the expected location of Proxima c strongly depends on the orbit inclination. The most reasonable counter-identifications are at sep = 802 and 767 mas and PA = 218.7 and 225.2 degrees, with $S/N = 1.6$ and 3.1 for JD = 58 588 and 58 621, respectively. This is further from the star than expected for an inclination of 120 degrees and suggests a lower inclination of the orbit. However, there are other peaks in the images of comparable strength, although these are incompatible with the orbit of Proxima c. Again, this underlines that we are unable to have unambiguous identification of the counterpart of Proxima c on any single epoch.

Using all epochs but 2017 (that is very uncertain; see Table 2), we may look for an eccentric orbit solution. We assumed that position errors are equal to 0.04/S/N arcsec (Zurlo et al. 2014) and ran the ORBIT fitting code by Tokovinin (2016)[1] that is based on a Levenberg-Marquard optimization algorithm to find the best astrometric orbit. The best solution (see Fig. 5) has a period of $P = 5.08 \pm 0.34$ yr, T0 = 2015.56 ± 0.22, eccentricity $e = 0.080 \pm 0.044$, semimajor axis $a = 1.02 \pm 0.06$ arcsec, the angle of descending node $\Omega = 150 \pm 7$ degrees, the argument of periastron $\omega = -2 \pm 34$ degrees, and $i = 137.3 \pm 6.2$ degrees, with a reduced $\chi^2 = 1.35$. This orbit agrees well with that from RVs (see Table 3)[2].

[1] https://zenodo.org/record/61119#.Xg83GxvSJ24

[2] The mass of Proxima given by this orbit is $M = 0.091 \pm 0.012\ M_\odot$, to be compared with the value of $0.12 \pm 0.02\ M_\odot$ given by Mann et al. (2015), that was adopted when determining the best circular orbit from 2018 data alone (Sect. 3.2). The lower value for the mass corresponding to the eccentric orbit is correlated to its lower inclination. However, the difference with the value given by Mann et al. (2015), is within the respective error bars.

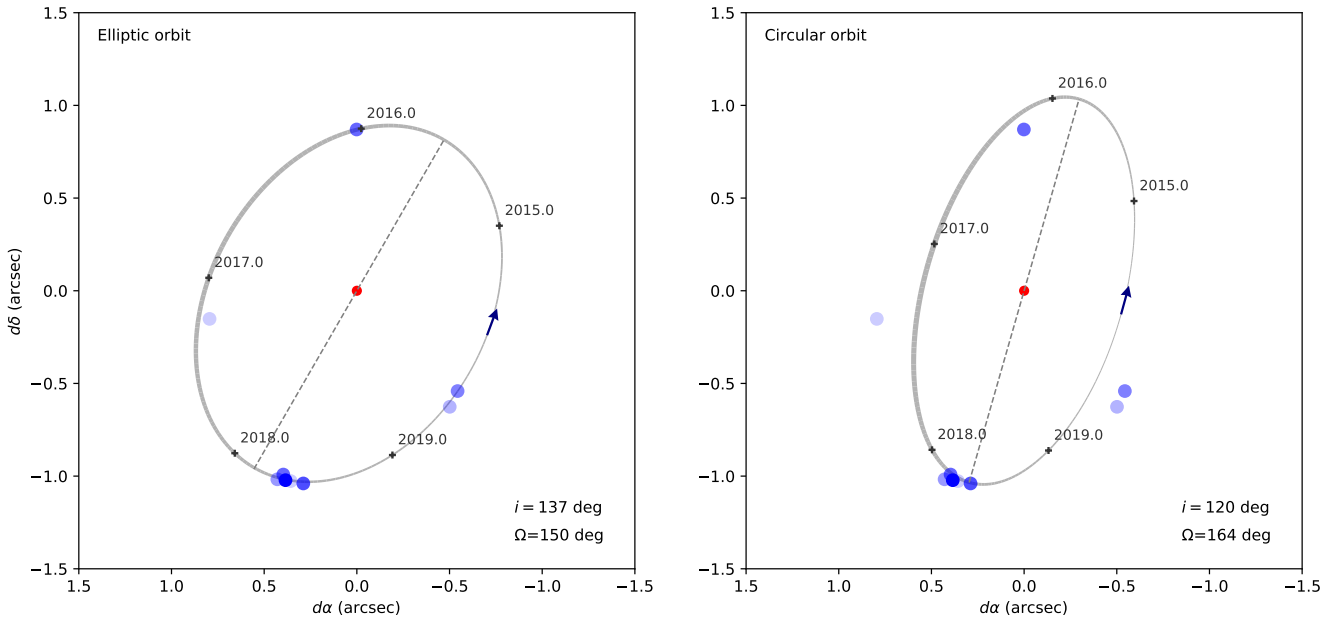

Fig. 5. Comparison between the proposed orbits for the candidate counterpart of Proxima c and the observations listed in Table 2. The density of the blue color of the points is proportional to the S/N in the individual epochs. *Left panel*: eccentric orbit. *Right panel*: circular orbit.

We note that while the orbital inclinations obtained using the circular and eccentric approach appear inconsistent with each other, this is not a real difference. The circular solution assumes the mass of the star, information from RVs (the range of semimajor axis and the phase), and only the astrometric data for 2018. It was important in this work to reproduce the apparent speed of Proxima c candidate projected on sky during this epoch. This speed can be obtained using a high inclination, but it can also be reproduced using a lower inclination but a lower stellar mass and/or assuming an eccentric orbit, in which the 2018 observations are acquired not far from apoastron. There is a degeneracy in this astrometric solution that can be broken using a wider set of measurements (2016, 2018, and 2019), which incidentally provides a dynamical estimate of the mass of Proxima and does not use RVs. The assumption of a circular orbit is however crucial in our analysis to have a first guess for the PA on sky and to estimate the probability that the detection of Proxima c candidate is a false alarm due to a random alignment of noise peaks.

While these are all reasonable explanations, we still think that the result is ambiguous and stress the need for further observations (direct imaging, RVs, and astrometry) to set the counter-identification of Proxima c on more solid basis.

4. Discussion

4.1. Mass and luminosity of Proxima c candidate

With an inclination of $i = 120$ degrees (circular orbit), the mass of Proxima c candidate from the spectroscopic orbit would be $7.2 \pm 2.2\ M_\oplus$; if the inclination is $i = 137.3$ degrees (eccentric orbit), the mass is $8.6 \pm 2.8\ M_\oplus$.

The average contrast measured for the candidate of Proxima c from SPHERE images is $(3.5 \pm 2.0) \times 10^{-7}$, that is about three times fainter than the upper limit found by Mesa et al. (2017). Intrinsic emission is surely negligible at the age of Proxima (4.8 Gyr; Thévenin et al. 2002; Bazot et al. 2016; Kervella et al. 2017); the planet should have a mass of about 5 $M_{\rm Jupiter}$ to be so bright, using AMES-COND models (Allard et al. 2011). We can then focus on the reflected star light. In this case, the contrast is written as

$$c = \phi A\ r^2/(4\ d^2), \tag{1}$$

where A is the albedo, r is the radius of the planet, d the distance from the star (1.3 au $= 2 \times 10^8$ km), and $0 < \phi < 1$ a parameter that takes into account the fractional illumination and scattering function along the orbit and depends on orbital inclination and phase. Hence, the observed contrast implies a radius of

$$r = 2\ d\ \sqrt{c/(\phi A)} = 4E8\ \sqrt{(3.5 \pm 2.0) \times 10^{-7}/(\phi A)}. \tag{2}$$

If $\phi A \sim 0.5$, we obtain $r \sim (3.4 \pm 1.2) \times 10^5$ km, that is about $4.8 \pm 1.7\ R_{\rm Jupiter}$. This is at least an order of magnitude too large for a Neptunian planet with a mass of 5–11 $M_\oplus$. However such a large size is possible for a system of rings or dust clouds around the planet; a similar explanation has been considered for Fomalhaut b (Kalas et al. 2008; Kennedy & Wyatt 2011; Currie et al. 2012; Janson et al. 2012; Tamayo 2014); see however Galicher et al. (2013) and Lawler et al. (2015) for a different interpretation of Fomalhaut b, and Kalas (2018) for a more recent discussion.

In this context, as long as our detection of Proxima c is not spurious, we note that it appears unresolved in SPHERE images, with a FWHM of ~35 mas, yielding an upper limit of about 120 $R_{\rm Jupiter}$ to the emitting area of the dust cloud. This value is consistent with the Hill radius (expected to be 39 ± 2 mas) and with the size of satellite systems of giant planets in the solar system. Furthermore, the dynamical mass for Proxima c candidate provided by RVs makes it consistent with the minimum mass (a few $M_\oplus$) required for exciting the collisional cascade in the swarming satellites scenario considered by Kennedy & Wyatt (2011). Similar information is not available for Fomalhaut b.

On the other hand, the age of Proxima (4.8 Gyr; Thévenin et al. 2002; Bazot et al. 2016; Kervella et al. 2017) is similar to that of the Sun and much older than Fomalhaut (440 ± 40 Myr; Mamajek 2012). For what we know at present, Proxima possibly contains only one long period planet, to be compared with

the four giant planets of the solar system, so that a planetary system around Proxima might be dynamically less evolved than the solar system. However, at present we cannot be sure about this. When compared to the Saturn ring system, the required disk system has a radius of ~5 $R_{\rm Jupiter}$ or larger, while the bright portion of the Saturn rings (rings B and A) extends up to about 2 $R_{\rm Jupiter}$, and the tenuous E-ring extends up to almost 7 $R_{\rm Jupiter}$. So the disk system required to explain the observation of Proxima c candidate should be likely larger than that of Saturn, but not by orders of magnitude. It is not known why there are disks or ring systems around old planets, and hence it is difficult to estimate the likelihood of observing these disks or ring systems around a putative Proxima c. In the case of Saturn, mainly two scenarios are considered in the literature. In the first scenario, the rings are residuals of an original much more massive disk that formed early in the system, either at formation or during late heavy bombardment (Canup 2010; Charnoz et al. 2011). In the second, largely based on the results of the Cassini mission, the rings are temporary features that can live a few hundred million years and they are then relatively young (Ida 2019; Iess et al. 2019). Still they are created after collisions and disruptions of massive bodies, which would be more probable in the early phases of the solar system evolution (Kerr 2008), but it is not clearly impossible at older ages. As a reference of the size of the bodies involved, the mass of Saturn's rings is estimated to be roughly half the mass of Mimas (Iess et al. 2019), which has a radius of about 200 km.

4.2. Comparison with Gaia results

If Proxima c exists, it should be detectable with the next *Gaia* data releases (see Damasso et al. 2020). Given the planet (5–11 $M_\oplus$) and host ($0.12 \pm 0.02\ M_\odot$, Mann et al. 2015) masses and the semimajor axis of the orbit (1.01 ± 0.05 arcsec), the astrometric signal should be ~200 μas and have a period of 5.2 yr. This is well above the detection limit of *Gaia*[3].

In the meantime, we may compare our proposed orbit with the astrometric signal that is obtained using *Gaia* DR2. The evidence for companions to Proxima on this data has been explored by Kervella et al. (2019) and by Brandt (2018, 2019)[4], who obtained consistent results. In the following, we consider more specifically the results obtained by Kervella et al. (2020; similar result are obtained by Benedict & McArthur 2020). By comparing the short-term proper motion vector measured by *Gaia* DR2 with the long-term trend derived using the *Gaia* DR2 and Hipparcos positions, Kervella et al. (2019) conclude that during the epoch surveyed by *Gaia* DR2 (2014 to 2016) Proxima exhibited a proper motion anomaly (hereafter PMa, compared to the long-term proper motion) of $d\mu_{\rm RA} = +0.22 \pm 0.11$ and $d\mu_{\rm Dec} = +0.38 \pm 0.21$ mas/yr, that is, toward the northeast. Since the mass ratio of Proxima to planet b is likely $>10^4$ and the maximum separation <40 mas, the reflex motion of Proxima around the barycenter has an amplitude of only <4 μarcsec. This is by far not enough to significantly affect the *Gaia* astrometry, so the observed PMa signal is entirely caused by planet c or additional massive long-period orbiting bodies.

While the error bars are still large, so that the significance of the PMa is only at a 1.8σ level, we may compare it with the prediction for the orbit we determined for the planet. We find that planet c moved toward NE with respect to Proxima during the *Gaia* DR2 time window (around J2015.5), at an average rate of $d\mu_{\rm RA} = +0.66$ and $d\mu_{\rm Dec} = +0.54$ arcsec yr^{-1}. Given the mass ratio of the planet to the star, this yields a PMa of $d\mu_{\rm RA} = -0.20$ and $d\mu_{\rm Dec} = -0.15$ mas yr^{-1} for Proxima. This is opposite from that found from the *Gaia* DR2 by Kervella et al. (2019, 2020). As a possible explanation of this difference of $\approx 3\sigma$, another massive planet may be orbiting Proxima with a longer period. Additional *Gaia* astrometric measurements are required to obtain a clear detection. The *Gaia* (E)DR3 will contain only time averaged PM values and not individual epochs (as the DR2). However, it should be possible from the combination of DR3 and DR2 to detect the signature of Proxima c (and putative additional bodies) at a significance level of more than 3σ.

4.3. Comparison with ALMA results

The inclination ($|i| = -60$ degrees) and PA of the circular orbit given by this candidate optical counterpart (162 degrees) are not too far (misalignment <30 degrees) from those proposed for the outer belt at ~30 au (inclination of 45 degree and PA of 140 degree) and for the cold ring (deconvolved size of ~0.8 au, PA ~ 130 degrees) proposed by Anglada et al. (2017) from ALMA 12 m array data. The agreement is even better (misalignment of 14 degrees, with a probability of chance alignment of ~3%) if we consider the tentative eccentric orbital plane ($\Omega = 150 \pm 7$ degrees, and $|i| = 42.7 \pm 6.2$ degrees). This is remarkable in view of the uncertainties in both estimates. However, it is possible that the orbit of c is not exactly coplanar with the outer belt and cold ring.

Anglada et al. (2017) also propose a secondary source from the ALMA 12 m array data at a separation of 1.2 arcsec and PA = 114 degree, at MJD = 57869. For comparison, our candidate counter-identification of Proxima c is at 1.08 arcsec and PA = 158.4 degrees at MJD = 58222. The question naturally arises of whether they could be the same object. Assuming our proposed circular (values in parenthesis are for the eccentric) orbit, we expect that the Proxima c candidate to be at sep = 0.59 (0.91) arcsec and PA = 100 (108) degrees at the epoch of the observation by Anglada et al. (2017). Given that the ALMA beam during this observation was 0.7 arcsec and that we have an uncertainty of 6 degrees in the PA of the circular orbit, the PA difference of 14 degree (6 degree for the eccentric orbit) is well within the uncertainties. The probability that this alignment is obtained by chance is 3.9% for the result of the circular orbit and 1.7% for that of the eccentric orbit. On the other hand, the expected separation of Proxima c candidate at the epoch of Anglada et al. (2017) observation is lower than that found on the ALMA data for both circular and eccentric orbits (in this second case, by only ~0.3 arcsec). Anglada et al. (2017) discuss the possibility that the emission observed by ALMA 12 m array results from a ring containing some $10^{-5}\ M_\oplus$ of dust around a planet, and cite theoretical arguments that the planet should be 10^7 times more massive (Charnoz et al. 2018); this is about ten times larger than the putative case of Proxima c. Given the large size and mass, it is possible that these counterparts to the RV signal are due to a ring or a debris disk, or it could be also a post-collisional disk (planet–planet collision). Alternatively, dust

[3] See https://www.cosmos.esa.int/web/Gaia/science-performance

[4] The saturation with *Gaia* starts around $G = 12$ (Evans et al. 2018), while Proxima has $G = 9$. The star is relatively faint in the visible, but its flux in the red is higher and the *Gaia* filter is very broad. This level of flux ($G = 9$) does not pose particular problems with the *Gaia* astrometry. This is shown by the RUWE (renormalized unit weight error) of Proxima that is equal to 1.0 (Kervella et al. 2019), which is in the reliable range (<1.4). This shows that the star is behaving correctly compared to other stars of similar brightness.

around Proxima c could be generated by collisional evolution of satellite swarms (Kennedy & Wyatt 2011).

It is also possible that the millimeter emission detected by Anglada et al. (2017) could be a cometary tail consisting of small size particles driven by the stellar wind. This might not be unexpected given the high level of activity of Proxima (see, e.g., Garraffo et al. 2016; Ribas et al. 2017; MacGregor et al. 2018; Howard et al. 2018) and the possible presence of dust around the companion.

Finally, it is also possible that the emission observed by Anglada et al. (2017) has a very different explanation. For instance, it may be a background source, such as a distant galaxy, although the probability of observing such a source at 1.2 arcsec from Proxima is $\leq 10^{-2}$ (Fujimoto et al. 2016; Anglada et al. 2017). Also, current data cannot completely rule out the possibility that it is just a noise peak. Further observations are clearly needed to clarify this subject.

5. Conclusions

While we are not able to provide a firm detection of Proxima c, we found a possible candidate that has a rather low probability of being a false alarm. If our direct near-infrared–optical detection of Proxima c is confirmed, it would be the first optical counterpart of a planet discovered from RVs; we note that the comparison with early *Gaia* results indicates that we should use extreme caution in reporting this detection. A dedicated survey to look for RV planets with SPHERE leads to nondetections (Zurlo et al. 2018b). If real, the detected object (contrast of about 16–17 mag in the H band) is clearly too bright to be the RV planet seen based on its intrinsic emission; this might then be circumplanetary material shining through reflected star-light. In this case we envision either a conspicuous ring system (Arnold & Schneider 2004), dust production by collisions within a swarm of satellites (Kennedy & Wyatt 2011; Tamayo 2014), or evaporation of dust boosting the planet luminosity (see, e.g., Wang & Dai 2019). This would be unusual for extrasolar planets, where Fomalhaut b (Kalas et al. 2008), for which there is no dynamical mass determination, is the only other possible example. Proxima c candidate is then ideal for follow-up with RVs observations, near IR imaging, polarimetry, and millimetric observations. As a consequence of the strong interest among the community and the public (see Proxima b, and the Breakthrough Starshot program; Kipping 2017 and its erratum Kipping 2018), the confirmation would be an important achievement for the field.

In addition, we note that if our detection is true, and the orbit of b is coplanar with that of c, which is consistent with the small misalignment between the best orbit for c and the outer belt revealed by ALMA (Anglada et al. 2017), the mass of Proxima b would be about 1.5–1.8 $M_\oplus$. An inclination of $|i| = 42-60$ degrees should not lead to transits of b (in agreement with observations of Feliz et al. 2019) for any reasonable value of the planet radius. Given the potential relevance of this work and its possible influence on the future detection of b, this work should be confirmed quickly with new high-contrast observations.

Acknowledgements. R.G., D.M., S.D., and M.D. acknowledge financial support from Progetto Premiale 2015 FRONTIERA (OB.FU. 1.05.06.11) funding scheme of the Italian Ministry of Education, University, and Research. A.Z. acknowledges support from the CONICYT + PAI/ Convocatoria nacional subvención a la instalación en la academia, convocatoria 2017 + Folio PAI77170087. E.R. and R.L. are supported by the European Union's Horizon 2020 research and innovation programme under the Marie Skłodowska-Curie grant agreement No 664931. J.H. is supported by the Swiss National Foundation (SNSF) for this work through the #*PZ*00$P2_1$80098 grant. This work has been supported by the project PRIN INAF 2016 The Cradle of Life - GENESIS-SKA (General Conditions in Early Planetary Systems for the rise of life with SKA). The authors acknowledge financial support from the Programme National de Planétologie (PNP) and the Programme National de Physique Stellaire (PNPS) of CNRS-INSU. This work has also been supported by a grant from the French Labex OSUG2020 (Investissements d'avenir - ANR10 LABX56). The project is supported by CNRS, by the Agence Nationale de la Recherche (ANR-14-CE33-0018). This work is partly based on data products produced at the SPHERE Data Centre hosted at OSUG/IPAG, Grenoble. We thank P. Delorme and E. Lagadec (SPHERE Data Centre) for their efficient help during the data reduction process. SPHERE is an instrument designed and built by a consortium consisting of IPAG (Grenoble, France), MPIA (Heidelberg, Germany), LAM (Marseille, France), LESIA (Paris, France), Laboratoire Lagrange (Nice, France), INAF Osservatorio Astronomico di Padova (Italy), Observatoire de Genève (Switzerland), ETH Zurich (Switzerland), NOVA (Netherlands), ONERA (France) and ASTRON (Netherlands) in collaboration with ESO. SPHERE was funded by ESO, with additional contributions from CNRS (France), MPIA (Germany), INAF (Italy), FINES (Switzerland) and NOVA (Netherlands). SPHERE also received funding from the European Commission Sixth and Seventh Framework Programmes as part of the Optical Infrared Coordination Network for Astronomy (OPTICON) under grant number RII3-Ct-2004-001566 for FP6 (2004-2008), grant number 226604 for FP7 (2009-2012), and grant number 312430 for FP7 (2013-2016). This work is supported by the French National Research Agency in the framework of the Investissements d'Avenir program (ANR-15-IDEX-02), through the funding of the "Origin of Life" project of the Univ. Grenoble-Alpes.

References

Allard, F., Homeier, D., & Freytag, B. 2011, ASP Conf. Ser., 448, 91
Amara, A., & Quanz, S. P. 2012, MNRAS, 427, 948
Anglada-Escudé, G., Amado, P. J., Barnes, J., et al. 2016, Nature, 536, 437
Anglada, G., Amado, P. J., Ortiz, J. L., et al. 2017, ApJ, 850, L6
Arnold, L., & Schneider, J. 2004, A&A, 420, 1153
Bazot, M., Christensen-Dalsgaard, J., Gizon, L., & Benomar, O. 2016, MNRAS, 460, 1254
Benedict, G. F., & McArthur, B. E. 2020, Res. Notes Am. Astron. Soc., 4, 46
Benedict, G. F., McArthur, B., Chappell, D. W., et al. 1999, AJ, 118, 1086
Beuzit, J. L., Vigan, A., Mouillet, D., et al. 2019, A&A, 631, A155
Brandt, T. D. 2018, ApJS, 239, 31
Brandt, T. D. 2019, ApJS, 241, 39
Canup, R. M. 2010, Nature, 468, 943
Charnoz, S., Crida, A., Castillo-Rogez, J. C., et al. 2011, Icarus, 216, 535
Charnoz, S., Canup, R. M., Crida, A., & Dones, L. 2018, in Planetary Ring Systems, Properties, Structure, and Evolution, eds. M. S. Tiscareno, & C. D. Murray (Cambridge: Cambridge University Press), 517
Claudi, R. U., Turatto, M., Gratton, R. G., et al. 2008, SPIE Conf. Ser., 7014, 70143E
Currie, T., Debes, J., Rodigas, T. J., et al. 2012, ApJ, 760, L32
Damasso, M., & Del Sordo, F. 2017, A&A, 599, A126
Damasso, M., Del Sordo, F., Anglada-Escudé, G., et al. 2020, Sci. Adv., 6, 7467
Delorme, P., Meunier, N., Albert, D., et al. 2017, in SF2A-2017: Proceedings of the Annual meeting of the French Society of Astronomy and Astrophysics, eds. C. Reylé, P. Di Matteo, F. Herpin, E. Lagadec, A. Lançon, Z. Meliani, & F. Royer, Di
Dohlen, K., Langlois, M., Saisse, M., et al. 2008, SPIE Conf. Ser., 7014, 70143L
Evans, D. W., Riello, M., De Angeli, F., et al. 2018, A&A, 616, A4
Feliz, D. L., Blank, D. L., Collins, K. A., et al. 2019, AJ, 157, 226
Fujimoto, S., Ouchi, M., Ono, Y., et al. 2016, ApJS, 222, 1
Gaia Collaboration (Brown, A. G. A., et al.) 2018, A&A, 616, A1
Galicher, R., Marois, C., Zuckerman, B., & Macintosh, B. 2013, ApJ, 769, 42
Garraffo, C., Drake, J. J., & Cohen, O. 2016, ApJ, 833, L4
Howard, W. S., Tilley, M. A., Corbett, H., et al. 2018, ApJ, 860, L30
Ida, S. 2019, Science, 364, 1028
Iess, L., Militzer, B., Kaspi, Y., et al. 2019, Science, 364, aat2965
Janson, M., Carson, J. C., Lafrenière, D., et al. 2012, ApJ, 747, 116
Kalas, P. G. 2018, Handbook of Exoplanets (Berlin: Springer International Publishing AG, part of Springer Nature), 38
Kalas, P., Graham, J. R., Chiang, E., et al. 2008, Science, 322, 1345
Kennedy, G. M., & Wyatt, M. C. 2011, MNRAS, 412, 2137
Kerr, R. A. 2008, Science, 319, 21
Kervella, P., Thévenin, F., & Lovis, C. 2017, A&A, 598, L7
Kervella, P., Arenou, F., Mignard, F., & Thévenin, F. 2019, A&A, 623, A72
Kervella, P., Arenou, F., & Schneider, J. 2020, A&A, 635, L14
Kipping, D. 2017, AJ, 153, 277
Kipping, D. 2018, AJ, 155, 103
Lawler, S. M., Greenstreet, S., & Gladman, B. 2015, ApJ, 802, L20

Le Coroller, H., Nowak, M., Arnold, L., et al. 2015, in Twenty Years of Giant Exoplanets, eds. I. Boisse, O. Demangeon, F. Bouchy, & L. Arnold (France: Observatoire de Haute-Provence), 59
Le Coroller, H., Nowak, M., Delorme, P., et al. 2020, ArXiv e-prints [arXiv:2004.12878]
Lovis, C., Snellen, I., Mouillet, D., et al. 2017, A&A, 599, A16
Lurie, J. C., Henry, T. J., Jao, W.-C., et al. 2014, AJ, 148, 91
MacGregor, M. A., Weinberger, A. J., Wilner, D. J., Kowalski, A. F., & Cranmer, S. R. 2018, ApJ, 855, L2
Mamajek, E. E. 2012, ApJ, 754, L20
Mann, A. W., Feiden, G. A., Gaidos, E., Boyajian, T., & von Braun, K. 2015, ApJ, 804, 64
Marois, C., Lafrenière, D., Doyon, R., Macintosh, B., & Nadeau, D. 2006, ApJ, 641, 556
Mawet, D., Milli, J., Wahhaj, Z., et al. 2014, ApJ, 792, 97
Mawet, D., Hirsch, L., Lee, E. J., et al. 2019, AJ, 157, 33
Mesa, D., Gratton, R., Zurlo, A., et al. 2015, A&A, 576, A121
Mesa, D., Zurlo, A., Milli, J., et al. 2017, MNRAS, 466, L118
Nowak, M., Le Coroller, H., Arnold, L., et al. 2018, A&A, 615, A144
Pavlov, A., Möller-Nilsson, O., Feldt, M., et al. 2008, SPIE Conf. Ser., 7019, 701939
Ribas, I., Gregg, M. D., Boyajian, T. S., & Bolmont, E. 2017, A&A, 603, A58
Showalter, M. R., de Pater, I., Lissauer, J. J., & French, R. S. 2019, Nature, 566, 350
Snellen, I., de Kok, R., Birkby, J. L., et al. 2015, A&A, 576, A59
Soummer, R., Pueyo, L., & Larkin, J. 2012, ApJ, 755, L28
Tamayo, D. 2014, MNRAS, 438, 3577
Thévenin, F., Provost, J., Morel, P., et al. 2002, A&A, 392, L9
Tokovinin, A. 2016, ApJ, 831, 151
van Leeuwen, F. 2007, A&A, 474, 653
Vigan, A., Moutou, C., Langlois, M., et al. 2010, MNRAS, 407, 71
Wang, L., & Dai, F. 2019, ApJ, 873, L1
Zurlo, A., Vigan, A., Mesa, D., et al. 2014, A&A, 572, A85
Zurlo, A., Gratton, R., Mesa, D., et al. 2018a, MNRAS, 480, 236
Zurlo, A., Mesa, D., Desidera, S., et al. 2018b, MNRAS, 480, 35

[1] INAF – Osservatorio Astronomico di Padova, Italy
e-mail: raffaele.gratton@inaf.it
[2] Núcleo de Astronomía, Facultad de Ingeniería y Ciencias, Universidad Diego Portales, Av. Ejercito 441, Santiago, Chile
[3] Escuela de Ingeniería Industrial, Facultad de Ingeniería y Ciencias, Universidad Diego Portales, Av. Ejercito 441, Santiago, Chile
[4] Aix-Marseille Université, CNRS, LAM (Laboratoire d'Astrophysique de Marseille) UMR 7326, 13388 Marseille, France
[5] INAF – Osservatorio Astrofisico di Torino, Italy
[6] Institute of Astrophysics, FORTH, GR-71110 Heraklion, Greece
[7] Department of Physics, University of Crete, 70013 Heraklion, Greece
[8] CRAL, UMR 5574, CNRS, Université Lyon 1, ENS, 9 avenue Charles André, 69561 Saint Genis Laval Cedex, France
[9] European Southern Observatory, Alonso de Cordova 3107, Casilla 19001 Vitacura, Santiago 19, Chile
[10] Univ. Grenoble Alpes, CNRS, IPAG, 38000 Grenoble, France
[11] Unidad Mixta Internacional Franco-Chilena de Astronomía, CNRS/INSU UMI 3386 and Departamento de Astronomía, Universidad de Chile, Casilla 36-D, Santiago, Chile
[12] Observatoire de Genève, Université de Genève, 51 Chemin des Mailletes, 1290 Sauverny, Switzerland
[13] Université Côte d'Azur, OCA, CNRS, Lagrange, France
[14] LESIA, Observatoire de Paris, Université PSL, CNRS, Sorbonne Université, Univ. Paris Diderot, Sorbonne Paris Cité, 5 place Jules Janssen, 92195 Meudon, France
[15] Max Planck Institute for Astronomy, Königstuhl 17, 69117 Heidelberg, Germany
[16] Department of Astronomy, Stockholm University, Stockholm, Sweden
[17] INAF – Osservatorio Astronomico di Brera, Milano, Italy
[18] STAR Institute, Université de Liège, Allée du Six Août 19c, 4000 Liège, Belgium
[19] Department of Astronomy, University of Michigan, 1085 S. Univer-sity Ave, Ann Arbor, MI 48109-1107, USA
[20] ONERA (Office National d'Etudes et de Recherches Aérospatiales), BP72, 92322 Chatillon, France
[21] Hamburger Sternwarte, Gojenbergsweg 112, 21029 Hamburg, Germany
[22] Center for Theoretical Astrophysics and Cosmology, Institute for Computational Science, University of Zürich, Zürich, Switzerland
[23] INAF – Osservatorio Astrofisico di Arcetri, Largo E. Fermi 5, 50125 Firenze, Italy
[24] European Southern Observatory, Karl-Schwarzschild-Strasse 2, 85748 Garching, Germany